Journal of Molecular Graphics and Modelling 29 (2011) 624–634

Contents lists available at ScienceDirect

Journal of Molecular Graphics and Modelling

journal homepage: www.elsevier.com/locate/JMGM

Understanding the effects of carbocyclic sugars constrained to north and south conformations on RNA nanodesign

Taejin Kim[a], Joseph J. Barchi Jr.[b], Victor E. Marquez[b], Bruce A. Shapiro[a,*]

[a] Center for Cancer Research Nanobiology Program (CCRNP), National Cancer Institute at Frederick, Frederick, MD, USA
[b] Laboratory of Medicinal Chemistry, National Cancer Institute at Frederick, Frederick, MD, USA

ARTICLE INFO

Article history:
Received 2 September 2010
Received in revised form 5 November 2010
Accepted 10 November 2010
Available online 19 November 2010

Keywords:
RNA
North constrained sugar
South constrained sugar
Molecular dynamics simulations
RNA structure deformations
RNA nanodesign

ABSTRACT

Relatively new types of the modified nucleotides, namely carbocyclic sugars that are constrained to north or south (C2′ or C3′ exo) conformations, can be used for RNA nanoparticle design to control their structures and stability by rigidifying nucleotides and altering the helical properties of RNA duplexes. Two RNA structures, an RNA dodecamer and an HIV kissing loop complex where several nucleotides were replaced with north or south constrained sugars, were studied by molecular dynamics (MD) simulations. The substituted south constrained nucleotides in the dodecamer widened the major groove and narrowed and deepened the minor groove thus inducing local conformational changes that resemble a B-form DNA helix. In the HIV kissing loop complex, north and south constrained nucleotides were substituted into flanking bases and stems. The modified HIV kissing loop complex showed a lower RMSD value than the normal kissing loop complex. The overall twist angle was also changed and its standard deviation was reduced. In addition, the modified RNA dodecamer and HIV kissing loop complex were characterized by principal component analysis (PCA) and steered molecular dynamics (SMD). PCA results showed that the constrained sugars stabilized the overall motions. The results of the SMD simulations indicated that as the backbone δ angles were increased by elongation, more force was applied to the modified RNA due to the constrained sugar analogues.

Published by Elsevier Inc.

1. Introduction

RNA based nanoparticle design has been recently studied for the purpose of developing drug delivery vehicles and therapeutic nanoparticles for tumor therapy [1]. One example of a designed small RNA structure is TectoRNAs, which were used to construct small (10 nm side length) and large (13 nm side length) tectosquares [2]. Tectosquares self-assemble by the interaction of kissing loops associated with a right angle motif and each tectosquare can then be used for constructing planar nanopatterns by specific sticky tail connectors. Other unique examples of RNA nanoparticles are the RNA hexagonal nanoring, RNA nanotube [3] and RNA cube [4]. The RNA hexagonal ring was made by the assembly of RNAIi and RNAIIi kissing loops having a 120° corner angle. Compared to tectosquares, which can be expanded in a two-dimensional plane, the RNA hexagonal ring can potentially be used to build RNA nanotubes by stacking several RNA hexagonal rings along the tube axis. The mechanical and thermodynamic properties of the RNA hexagonal ring were studied by MD simulations, including elastic and transport coefficient determinations [5]. As another example, the pRNA (packaging RNA) of bacterial virus phi29 can form dimers, trimers, and hexamers and can be used as a drug delivery vehicle to load siRNA and other therapeutic molecules [1]. It is also possible to design a variety of different nanoparticles with the help of the unique software, NanoTiler [6]. NanoTiler can be used with the RNAJunction data base [7], which is designed to automatically detect RNA building blocks such as junctions, kissing loops, internal loops, etc, to build nano structures [2–4] from these building blocks by using algorithms for ring closure, sequence fusing, and sequence optimization. However, all the experimental and computational nanoparticle designs use unmodified nucleotides and these building block motifs are limited by the intrinsic architectural properties of normal nucleotides. In recent years, various scaffolds that effectively constrain nucleotide sugar pucker such as "locked" nucleic acids (LNA′s) [8] and [3.1.0]bicyclohexane systems [9–14] have proved quite useful in the design of oligonucleotides (ODN) with defined conformational properties [8,15–17]. Since these modified nucleotides can provide more geometric control and stability, they may open an entire new avenue of RNA nanoparticle design.

Most RNA structures (82%) in the protein data bank (PDB) which satisfy a minimum resolution of 3.0 Å have north (C3′ endo) sugar pucker conformations, while a small number (10%) of the sugar puckers have south (C2′ endo) conformations [18]. However, it is

* Corresponding author. Tel.: +1 301 846 5536; fax: +1 301 846 5598.
E-mail address: shapirbr@mail.nih.gov (B.A. Shapiro).

1093-3263/$ – see front matter. Published by Elsevier Inc.
doi:10.1016/j.jmgm.2010.11.007

possible to induce deformations and increase the stability of RNA structures by the use of modified sugar puckers [19–20]. Since modified nucleotides which have a north (or south) constrained sugar can lock the pseudo-rotational angle within the range of a north (south) conformation [9–14], they can induce a deformation in the nucleic acid helix. In one study, thymidine analogs containing north constrained [3.1.0]bicyclohexane sugars substituted into the central region of the palindromic Dickerson dodecamer DNA, d(CGCGAATTCGCG)$_2$ [17] proved to induce bending toward the major groove in the DNA helix. In both the NMR structures and the MD simulations, the structural bending was observed to depend on the number and the position of the substituted modified thymidine pairs. The local structure adjacent to the modified thymidine pairs also deformed into an A-form like helix [15,16]. A similar study was performed with LNA′s [8], that have an RNA-like sugar conformation (C3′ endo) induced by linking O2′ and C4′. Due to the strongly locked sugar, LNA–RNA, LNA–DNA and LNA–LNA duplexes [21–24] adopt an A-form helix geometry and, for example, about 50% of the sugar puckers of the DNA strand in the LNA–DNA hybrid maintained north conformations. Therefore, it is possible to use LNA to lock the sugar pucker in a north conformation and rigidify or induce deformations in RNA. However, since LNA can only be locked in the north sugar conformation and the 2′-hydroxyl is absent due to the O2′–C4′ linkage, the use of LNA′s presents limitations for studying RNA structures where north and south constrained sugars and 2′-hydroxyls are necessary for specific geometries and chemistries.

In this study, we examine the overall control of the structure and dynamics of RNAs imposed by the bicyclo[3.1.0]hexane structure of modified nucleosides constrained to either a north (Fig. 1(a)) or a south (Fig. 1(b)) conformation depending on the location of the fused cyclopropane ring. Since RNA duplexes and kissing loop structures are commonly used motifs in RNA nanoparticle assembly, we substituted modified nucleotides into a 12-mer dodecamer (5′-CGCGAAUUCGCG-3′, see Fig. 1(c)) and the kissing loop complex from the dimer initiation site (DIS) of the human immunodeficiency virus (HIV) to examine flexibility change and overall effect on helix parameters. In HIV-1, the conformations of the flanking purines A_{272} and A_{273} in subtype-B (Lai) in the X-ray structure are bulged-out and stacked in pairs forming open conformations (Fig. 1(e)). Both A_{271} and A_{273} in the X-ray structure have C2′-endo (south) conformations while all other sugars have C3′-endo (north) conformations. On the other hand, the flanking bases in the subtype-B NMR structure are between a bulged-in and a bulged-out conformation and stack in reverse compared to the X-ray structures (Fig. 1(f), reverse stacking). The only sugar pucker in a C2′-endo conformation in the NMR structure is A_{272}. Since the flanking base conformations of the X-ray structure can be affected by crystal packing, the effects of the modified nucleotides on the flanking bases in both the X-ray and the NMR structures are used in this paper. For these reasons, we studied the modified subtype-B HIV kissing loop structures of both the X-ray and the NMR structures using 30 ns explicit solvent molecular dynamics (MD) simulations and we observed a strong consistency in the flanking base behaviors that are dependent on the type and the location of the substituted modified nucleotides. In addition, trajectories from the 30 ns MD simulations were analyzed by principal component analysis (PCA). The top three principal components (PCs) of the dodecamers and both the X-ray and NMR HIV-1 kissing loop complexes show that the modified nucleotide substitutions are able to control the overall flexibility. Our steered molecular dynamics (SMD) simulations results also show the differences obtained from applied forces, which include the corresponding conformational changes from elongation between an unmodified and a modified structure. These results show that north and south constrained sugars can be used to induce appropriate structural changes and control flexibility of the RNA motif which can be important for RNA self-assembly and for RNA based nano applications to control shapes and chemical properties.

2. Methods

2.1. Initial structures of the unmodified and the modified RNA dodecamers and HIV-1 kissing loop complexes

A 12mer RNA palindromic dodecamer (5′-CGCGAAUUCGCG-3′) was prepared with Accelrys Discovery Studio®. A north modified dodecamer was obtained by substituting north modified nucleotides into all nucleotides in both strands except the 5′ and 3′ terminal ends. A south modified dodecamer was prepared by substituting south modified nucleotides into even nucleotides (2nd, 4th, 6th, 8th and 10th) in both strands. Therefore, the initial structures of both north and south modified dodecamers were A-form. For the HIV-1 kissing loop complexes, subtype-B X-ray (pdb code: 2B8R) and NMR (pdb code: 2F4X) structures were used. All ions were removed from the X-ray structure before they were neutralized with Na^+ ions. For both the X-ray and the NMR structures, north and south modified nucleotides were substituted at G_{271} and A_{273} to determine the effect of the modified nucleotides on the flanking base conformations and the overall dynamics. In addition, nucleotides in the stem regions were also replaced by north modified nucleotides to test the ability to control the flexibility of the stems. In order to specify each modified HIV kissing loop complex conveniently, we indicate the locations of the substituted modified nucleotides as subscripts of the type of modified nucleotide. For example, for the kissing loop complex $N_{271,273}$ signifies that north modified nucleotides were substituted at G_{271} and A_{273} (and the symmetrical ones, G_{271}* and A_{273}*). The modified dodecamers and the HIV-1 kissing loop complexes that were used for the MD simulations are listed in Table 1.

2.2. Force-field for molecular dynamics simulations

Amber antechamber [25] was used to assign atom and bond types to modified north and south nucleotides which contain north or south constrained carbocyclic sugars. Nucleic acid force fields of the modified nucleic acids were determined based on the atom and bond types. Dihedral force parameters for the north and south carbocyclic sugars were obtained from previous ab initio calculations [20]. These parameters were applied to the constrained carbocyclic sugars in the modified nucleotides after scaling. ab initio calculations were performed using the GAUSSIAN suite of programs [26] to compute the electrostatic potential (ESP). ESP was fit using restrained electrostatic potential (RESP) charge fitting [27] with antechamber and the resultant partial charges were used for the modified north and south nucleotides. Once all of the force fields were obtained for the modified north and south nucleic acids, molecular dynamics (MD) simulations were applied to the modified nucleotide sugar pucker to see if they maintained the proper sugar puckers (north and south) in explicit solvent. All simulations were performed using the ff99 Cornell force field [28] with the Amber 10 molecular dynamics (MD) simulation package [29].

2.3. Molecular dynamics simulations protocol

Once the modified nucleotides were substituted into the RNA dodecamer or HIV kissing loop complex, initial energy minimization was performed to remove bad atomic contacts. All minimized structures were neutralized by Na^+ ions using the LEAP module in Amber 10. A TIP3P water [30] box was added so that there was a 15 Å distance from each side of the solute. The electrostatic interactions

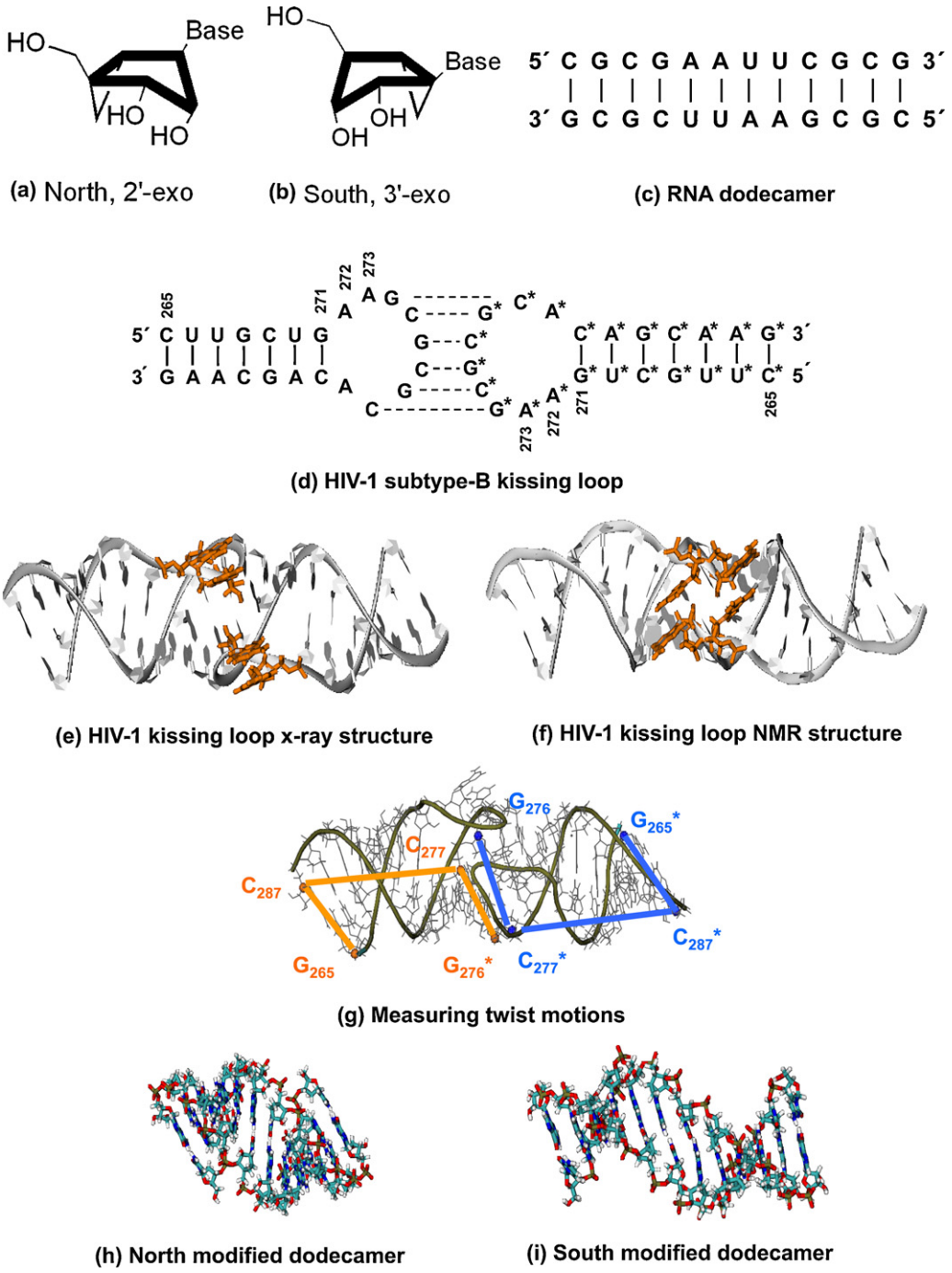

Fig. 1. The modified nucleoside which contains an embedded cyclopentane ring constrained in (a) north and (b) south conformations. Secondary structure of 12mer RNA dodecamer (c) and subtype-B HIV kissing loop complex (d). The symbol "*" in (d) indicates the other hairpin structure in the kissing loop complex and dashed lines between bases indicate kissing loop interactions. The conformations of the flanking purines A_{272} and A_{273} in subtype-B in the X-ray structure (e) are bulged-out and stacked in pairs forming open conformations while those in the NMR structure (f) are between a bulged-in and a bulged-out conformation (reverse stacking). (g) measuring twist angles of individual stems using the dihedral angle along the C4′ atoms of C_{265}, G_{287}, C_{277}, and G_{276}* and the corresponding dihedral angle on the other side. The average structure of (h) north modified dodecamer and (i) south modified dodecamer.

were calculated by particle mesh Ewald summation (PME) [31] and the non-bonded interactions were truncated at 9.0 Å. Overall minimization of the system was done using harmonic constraints on the RNA. This was followed by heating the system to 300K while constraining the solute with a 200 kcal/(mol Å) harmonic constraint. Constraints were slowly released while the system was equilibrated. During the 30 ns MD production run, a parabolic restraint on distance (3.0 Å, 10 kcal/(mol Å)) was applied to the hydrogen bonds in the 5′ and 3′ CG base pairs [8,15]. Since the restraint was applied only when the hydrogen bond distance was greater than 3.0 Å, which was found to be less than 0.2% of the whole simulation time, the applied restrained energy on the system was very small. SHAKE [32] was applied to all hydrogens to remove the fastest hydrogen vibrations and to allow longer simulation time steps. The pressure was maintained at 1.0 Pa and a constant temperature of 300 K was maintained using a weak-coupling algorithm [33]. A production simulation was performed for 30 ns with a 2 fs timestep.

2.4. Analysis methods, principal component analysis, and steered molecular dynamics

Since the motion of RNA motifs are important for RNA nanoparticle design and self-assembly, we monitored twisting motion, helix elongation and backbone dihedral angles. Total twist angle was determined by measuring the dihedral angle along the C4′ atoms of C_{265}, G_{287}, C_{265}*, and G_{287}* in the kissing loop complex. In addition, twist angles of individual stems were measured using the dihedral angle along the C4′ atoms of C_{265}, G_{287}, C_{277}, and G_{276}* and the corresponding dihedral angle on the other side (C4′ atoms at C_{265}*, G_{287}*, C_{277}*, and G_{276}) (see Fig. 1(g)). More precise information of overall dynamics was captured by applying principal component analysis (PCA). The effect of the substituted modified nucleotides was also measured with SMD simulations by stretching unmodified and north modified dodecamers and the kissing loop complexes along a helical axial direction. Each equilibrated RNA structure from the previous 30 ns simulations was immersed in a larger water box and equilibrated for 2 ns followed by the same protocol that was described before. SMD simulations were repeated five times for five different initial structures which were chosen from 2 ns MD simulations. In each SMD simulation, the O5′ and O3′ atoms on one end were fixed, while the O5′ and O3′ atoms at the other end were stretched at a constant speed of 1.0 Å/ps by a virtual harmonic spring with a spring constant of 6 kcal/mol Å^2 (=416 pN/Å). All SMD simulations were carried out using the NAMD software package with an Amber force field (ff99) and the parabolic restraints that were applied to the hydrogen bonds on the 5′ and 3′ CG base pairs were removed.

3. Results and discussion

3.1. Dynamics of the modified and the unmodified RNA dodecamers

3.1.1. RMSD of the unmodified and the modified dodecamers

The average RMSD values of the unmodified, north and south dodecamers from their starting structures and from the structure at 10 ns are listed at the bottom of Table 2 and their time variations are plotted in Fig. 2. As Fig. 2(a) indicates, the south modified dodecamer experiences larger deformations than the other two dodecamers in the range of 0–30 ns. However, in the range of 10–30 ns, the RMSD and the standard deviation of the south modified dodecamer are as low as that of the unmodified dodecamer (see Fig. 2(b)). The north modified dodecamer shows slightly improved RMSD values when compared to the unmodified dodecamer in the range of 10–30 ns. Therefore, the initial conformational changes

Table 1
Modification of RNA dodecamer and HIV kissing loop complexes by substitution of modified nucleotides.

Name of modification	Type and position of the modified nucleotides
North modified Dodecamer	North modified nucleotides in both strands except the 5′ and 3′ terminal ends
South modified Dodecamer	South modified nucleotides at 2nd, 4th, 6th, 8th and 10th nucleotides in both strands
$N_{271.273}$ (kissing loop)	North nucleotides at G_{271}, A_{273}, G_{271}*, A_{273}*
$S_{271.273}$ (kissing loop)	South nucleotides at G_{271}, A_{273}, G_{271}*, A_{273}*
N_{stems} (kissing loop)	North nucleotides in both stem regions

The name of the modified RNA structure, modified nucleotides, and the positions where the modified nucleotides are substituted. In the HIV-1 kissing loop complexes, the same modification is applied to both the X-ray and the NMR structures.

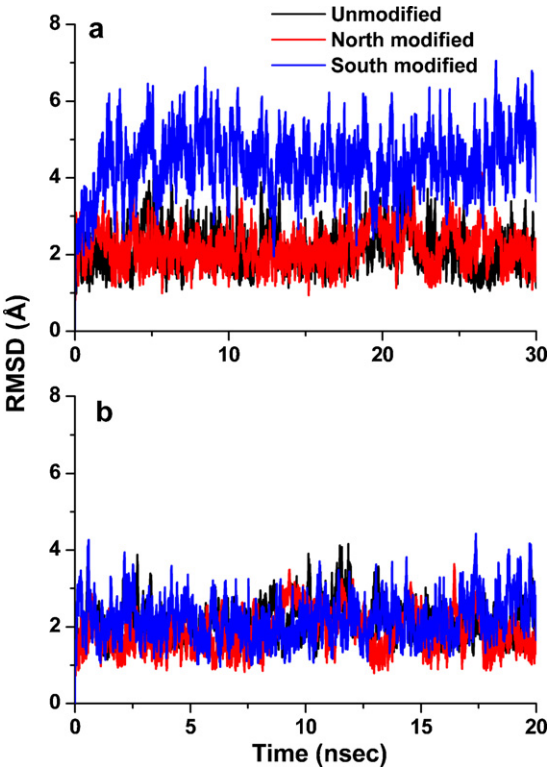

Fig. 2. The RMSDs of the unmodified, the north modified and the south modified dodecamers from (a) the initial structures and (b) the structure at 10 ns.

Table 2
Backbone dihedral angles, twist angles, total length, and RMSD's of the unmodified and the modified dodecamers.

		Unmodified dodecamer (A-Form)	North modified dodecamer	South modified dodecamer		DNA [39] (B-Form)
				Unmodified nucleotide	South modified nucleotide	
α		263.0 ± 9.5	267.7 ± 3.2	234.6 ± 17.8	273.4 ± 3.3	300
β		175.8 ± 3.5	178.8 ± 1.8	180.5 ± 3.5	182.1 ± 3.5	180
γ		82.5 ± 7.9	76.4 ± 2.7	95.6 ± 16.3	74.1 ± 2.5	55
δ		80.0 ± 1.9	74.4 ± 1.6	77.3 ± 4.1	145.6 ± 1.6	140
ε		201.1 ± 2.0	204.7 ± 1.8	197.7 ± 3.2	187.4 ± 3.0	190
ζ		291.1 ± 2.1	294.7 ± 2.0	283.0 ± 4.0	266.5 ± 4.0	260
χ		201.4 ± 2.7	192.8 ± 1.9	196.7 ± 3.4	228.9 ± 3.2	255
Twist angle (°)		−24 ± 14.6	−11.4 ± 15.6	−43.7 ± 10.5		
Total length (Å)		32 ± 2.3	29 ± 2.3	40 ± 2.2		
RMSD (Å)	0–30 ns	2.1 ± 0.5	2.2 ± 0.5	4.4 ± 0.8		
	10–30 ns	2.1 ± 0.4	1.8 ± 0.5	2.2 ± 0.5		

Average backbone dihedral angles between 10–30 ns. The 2nd and 3rd columns are the average backbone dihedral angles of the unmodified and the north modified dodecamers respectively. The 4th and 5th columns are the average backbone dihedral angles of the unmodified and the south modified nucleotides in the south modified dodecamer. The backbone dihedral angles of a B-form DNA (6th column) are from reference [39]. At the bottom of the table are twist angles, standard deviations, total average lengths and the RMSDs with respect to the initial and the structures at 10 ns.

induced by the substituted modified nucleotides fully disappear after 10 ns, and the flexibility of both modified dodecamers are as stable as that of the unmodified. On the other hand, even though their RMSD differences are small, the application of SMD simulations shows that the north dodecamer helix is stiffer than the unmodified case (see below).

3.1.2. Backbone angle and conformation change

The average backbone dihedral angles for the last 20 ns was calculated and is summarized in Table 2. Since the south modified dodecamer has both unmodified and south constrained sugars, the average backbone dihedral angles for each sugar group are calculated separately and listed in the 4th and 5th columns in Table 2. The overall helix in the unmodified and the north modified dodecamers maintain an A-form during the simulation. The average backbone dihedral angles in the north modified dodecamer show lower standard deviation values, which may explain the slightly lower RMSD values compared to the unmodified dodecamer. In the south modified dodecamer, the overall backbone dihedral angles in the unmodified nucleotides maintain an A-form, while those of the south modified nucleotides are similar to B-form DNA backbone dihedral angles. Compared to the backbone angles in the unmodified dodecamer (2nd column), the unmodified nucleotides in the south modified dodecamer (4th column) shows larger standard deviation values, while those of south modified nucleotides (5th column) are relatively stable. Larger δ angles in the south modified dodecamer cause an elongation of the overall length, which is measured between the center of mass of each of the terminal bases for the last 20 ns. The average distance between two phosphates in the backbone of a south constrained sugar is 7.2 Å, and its δ angle is 145°. On the other hand, the average distance between the phosphates with the unmodified sugars is 6.2 Å with a corresponding δ angle of 75°. Therefore, the average length of the south modified dodecamer (Fig. 1(i)) is elongated by 30% when compared to the unmodified and north modified dodecamers (see Fig. 1(h) and Table 2). In addition, the Curves program [34] shows that the major groove of the south modified dodecamer becomes wider and the minor groove becomes narrower and deeper.

The modified nucleotides in the dodecamers alter the overall twist motions. The average twist angle, which measures the dihedral angle along the C4′ atoms of C_1, G_{24}, C_{13}, and G_{12} and its variation (standard deviation) for the last 20 ns are summarized in Table 2. The north dodecamer has a smaller average twist angle when compared to the unmodified dodecamer. The variation in the twist angle for both the unmodified and the north modified dodecamers are about the same. On the other hand, the twist angle of the south dodecamer increases while its variation is reduced compared to the unmodified dodecamer.

3.2. Overall structure and dynamics of the HIV kissing loop

3.2.1. RMSD of the unmodified and the modified kissing loop complexes

The RMSDs of the unmodified and $N_{271.273}$ kissing loop complexes from their starting structure and from the structure at 10 ns are plotted in Fig. 3 (X-ray structure) and Fig. 4 (NMR structure). The average and standard deviation values of the RMSDs in the range of 10–30 ns are listed in Table 3. The RMSDs in both Figs. 3 and 4 show lower and more stable distributions for the modified structures compared to the unmodified kissing loop complexes in the range of 10–30 ns. RMSD distributions of other modified kissing loop complexes also show the same behavior (data not shown). From the RMSD values in Table 3, a strong consistency is observed between the X-ray and the NMR structures. In the modified kissing loop complexes, $N_{271.273}$ of both the X-ray and NMR structures show the lowest RMSD values, while $S_{271.273}$ of both structures

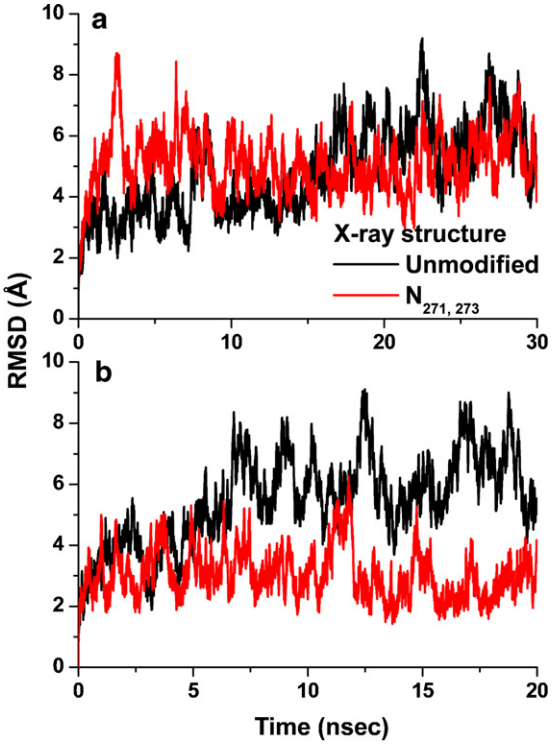

Fig. 3. The RMSDs of the X-ray structures of the unmodified and $N_{271.273}$ modified kissing loop complexes from (a) the initial structures and (b) the structure at 10 ns.

have the largest RMSD values. The RMSD and standard deviation of N_{stems} show the same lower values (3.0 ± 0.6 Å) for both the X-ray and NMR structures. Therefore, these results indicate that it is possible to reduce and to stabilize the overall RMSDs by substituting modified nucleotides into specific positions of the kissing loop complexes.

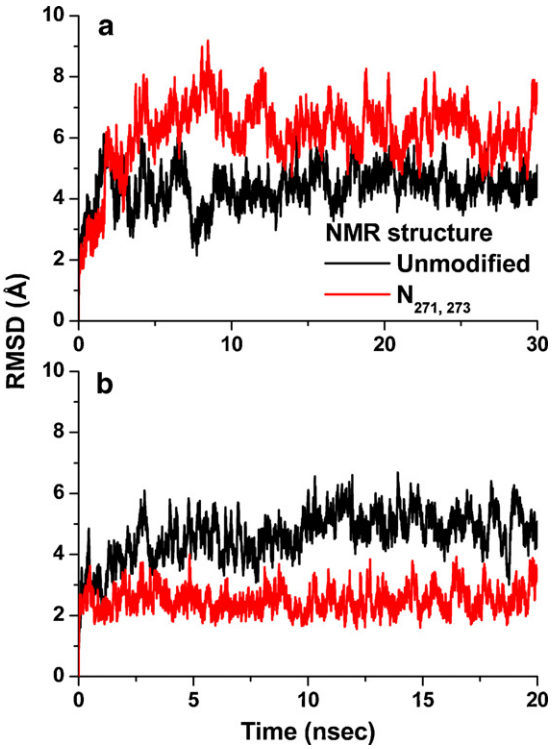

Fig. 4. The RMSDs of the NMR structures of the unmodified and $N_{271.273}$ modified kissing loop complexes from (a) the initial structures and (b) the structure at 10 ns.

Table 3
Flanking base conformations, twist angles and RMSD's of the unmodified and the modified kissing loop complexes.

Type	Flanking bases' formation in most of MD simulation time	Twist angle (degree)		RMSD (Å) (10–30 ns)
		Total	Individual stems	
		X-ray		
Unmodified	A_{272} (bulged-in) A_{273}, A_{272}*, A_{273}* (Bulged-out, stacked)	−78.3 ± 26.4	−44.6 ± 17.5 −52.1 ± 12.3	5.5 ± 1.5
$N_{271.273}$	A_{272},A_{273}, A_{272}*, A_{273}* (bulged-out, stacked)	−70.9 ± 18.0	−49.1 ± 12.5 −49.3 ± 12.7	3.0 ± 0.8
$S_{271.273}$	A_{272} and A_{273} (bulged-out) A_{272}*, A_{273}* (fluctuated between half bulged-in and bulged-out)	−69.1 ± 17.5	−50.0 ± 13.4 −46.5 ± 13.4	3.4 ± 0.6
N_{stems}	A_{272} and A_{273} (stacked, bulged-out) A_{272}* and A_{273}* (stacked, bulged-in)	−58.2 ± 25.7	−23.9 ± 14.0 −36.1 ± 15.0	3.1 ± 0.6
		NMR		
Unmodified	A_{272}, A_{272}* (bulged-in) A_{273}, A_{273}* (half bulged-out, stacked)	−54.2 ± 17.3	−45.9 ± 13.8 −24.3 ± 16.5	4.6 ± 0.8
$N_{271.273}$	All flanking bases bulged-out A_{272}, A_{272}*, A_{273} (stacked)	−113.1 ± 15.8	−51.1 ± 12.9 −78.0 ± 11.9	2.4 ± 0.4
$S_{271.273}$	A_{272} A_{272}*, A_{273}* (stacked, half bulged-in) A_{273} (bulged-out)	−113.7 ± 24.0	−59.8 ± 15.1 −60.5 ± 17.2	4.2 ± 0.8
N_{stems}	A_{272}, A_{272}* and A_{273} (bulged-in) A_{273}* (bulged-out)	−102.5 ± 18.6	−64.3 ± 17.8 −43 ± 13.0	3.0 ± 0.6

Brief description of flanking base conformations, total and individual twist angles with variations, and RMSDs between 10 and 30 ns from the structures at 10 ns.

3.2.2. *The behavior of the flanking bases (A_{272}, A_{273}, A_{272}*, and A_{273}*)*

The flanking bases in the unmodified X-ray structure maintain their initial conformation for the first 7.0 ns. Near 7.5 ns, A_{272} forms a bulged-in conformation and makes hydrogen bonds with other bases (A_{280}, C_{281} and G_{274}*) while the three other flanking bases (A_{273}, A_{272}*, and A_{273}*) are bulged-out and stacked. This conformation is maintained for the rest of the simulation (see Fig. 5(a)). A similar bulged-in behavior of the flanking bases is observed in the unmodified NMR structure. During the first 10 ns, the flanking bases maintain the initial conformation (reverse stacking). At 11 ns, A_{272} is bulged-in and establishes hydrogen bonds with A_{280}. At 17 ns, A_{272}* is bulged-in and establishes hydrogen bonds with A_{280}*. The other two flanking bases (A_{273}, A_{273}*) stack and lie down on the stem-2 side and hydrogen bond with A_{272}* or C_{280}* for short discrete time intervals (named half bulged-out). This conformation is maintained for the rest of the simulation (Fig. 5(b)).

Only in the presence of Mg^{2+} ions do the flanking bases of the subtype-B HIV kissing loop complex form a closed conformation (all flanking bases are bulged-out and stack together) for 13 ns in a 30 ns MD simulation [35]. Compared to this result, it is interesting to find that the north modified nucleotides at G_{271}, A_{273} ($N_{271.273}$) in the X-ray structure induce a closed conformation near 0.5 ns and maintain it for the rest of the simulation (29.5 ns) without Mg^{2+} ions (see Fig. 5(c)). The flanking bases in the NMR structure of $N_{271.273}$ also show a similar behavior even though their initial conformation is quite different from the X-ray structure. In less than 1 ns, A_{272} and A_{272}* bulge-out and stack on each other, while the other flanking bases maintain their initial conformation. At 8.5 ns, A_{273} bulges-out and stacks together with A_{272}, A_{272}*, while A_{273}* bulges-out without stacking. This conformation is maintained for the rest of the simulation (see Fig. 5(d)).

The south modified nucleotides at G_{271} and A_{273} ($S_{271.273}$) induce significantly different flanking base conformations compared to the previous cases. In the X-ray structure of $S_{271.273}$, A_{272}*, A_{273}* stack on each other and fluctuate between the half bulged-in and bulged-out conformations while A_{272} and A_{273} bulge-out without stacking. (see Fig. 5(e)). In the NMR structure of $S_{271.273}$, A_{272}*, A_{273}* and A_{272} are rotated into the kissing loop stacking together, and A_{272}* forms hydrogen bonds with A_{271} and C_{281} near 13 ns. The other flanking base, A_{273} remains bulged-out (see Fig. 5(f)). Therefore, the substitution of south constrained sugars at G_{271} and A_{273} fail to form a closed conformation.

When all nucleotides in both stems were replaced with the north modified nucleotides (N_{stems}), the flanking bases are not induced to form a closed conformation. In the X-ray N_{stems}, A_{272}* and A_{273}* form a bulged-in conformation while A_{272} and A_{273} bulge-out and stack (see Fig. 5(g)). In the NMR structure N_{stems}, A_{272}, A_{272}* and A_{273} stay in a bulged-in conformation while A_{273}* is bulged-out for most of the simulation time (see Fig. 5(h)).

3.2.3. *Twist motions in the unmodified and the modified kissing loop complexes*

As summarized in Table 3, the conformation of the flanking bases affect the individual and overall twist angles of the unmodified and the modified kissing loop complexes. In the X-ray structures, the average total twist angles of the modified kissing loop complexes are 10–20° smaller than the unmodified kissing loop complex. On the other hand, the modified NMR structure kissing loop complexes show about a 50° larger total average twist angle than the unmodified kissing loop complex. Besides the total twist angle change in each case, it is also important to consider the variation in the total twist angles, which determines the flexibility of the structure. The variations of the total twist angles in the $N_{271.273}$ of both the X-ray and the NMR structures are decreased compared to the corresponding unmodified kissing loop complexes. The variations of total twist angle in both the X-ray and the NMR N_{stems} are almost the same as the corresponding unmodified kissing loop complexes. This result is consistent with the north dodecamer, whose twist angle variation is almost the same as the unmodified dodecamer. The total twist angle variation of the $S_{271.273}$ in the X-ray structure is decreased, however, the NMR $S_{271.273}$ total twist angle variation is increased with respect to the corresponding unmodified kissing loop complex. Therefore, substituting modified flanking bases into specific positions can control the overall twist angle or the flexibility of the twist motion.

The individual twist angles of the stems and their variations (see Table 3) also show that the stability of twist motion depends on the flanking base conformations and their stability. When all the flanking bases are not involved in hydrogen bonds with other bases in the kissing loop or stems, individual twist angle variations induce uniform motion on both stems. Both the X-ray and the NMR

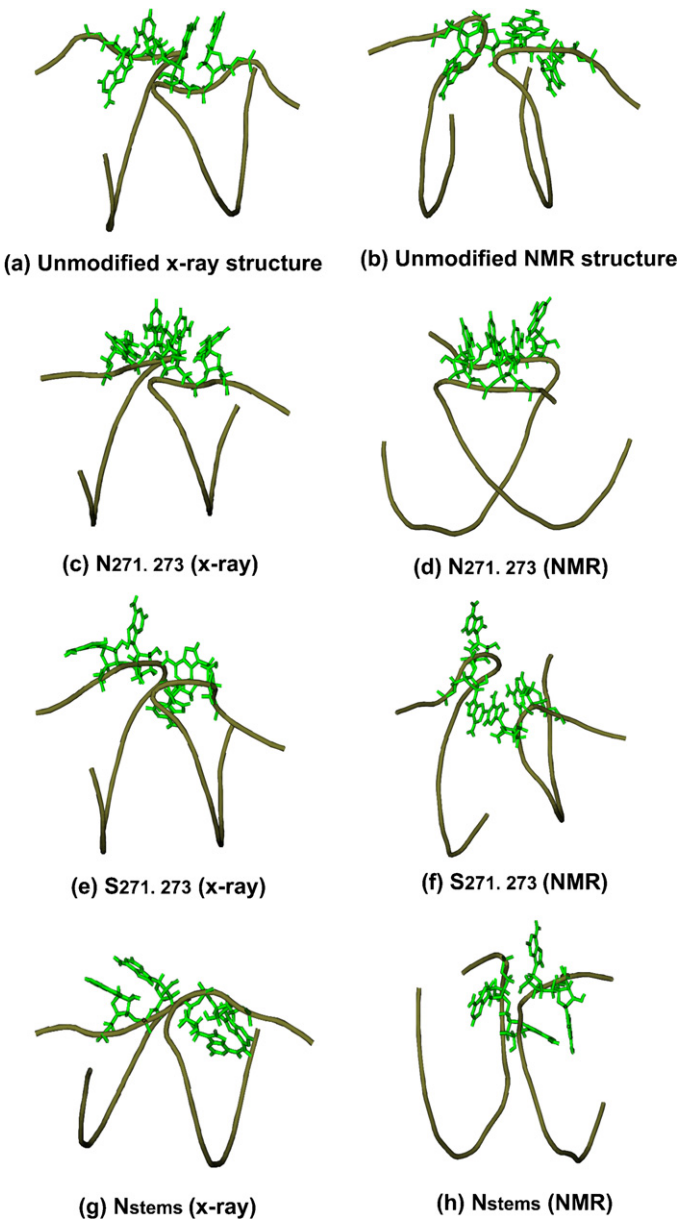

Fig. 5. Average position of flanking bases for (a) unmodified X-ray, (b) unmodified NMR, (c) $N_{271.273}$ (X-ray), (d) $N_{271.273}$ (NMR), (e) $S_{271.273}$ (X-ray), (f) $S_{271.273}$ (NMR), (g) N_{stems} (X-ray) and (h) N_{stems} (NMR). Only X-ray and NMR $N_{271.273}$ form bulged-out and stacked flanking base conformations.

$N_{271.273}$ as well as the X-ray $S_{271.273}$ show this behavior. In addition, when the flanking bases symmetrically form bulged-in or form stable hydrogen bonds, individual twist angle variations are similar for both stems. The X-ray N_{stems} structure belongs to this group. On the other hand, when the flanking bases bulge-in and form hydrogen bonds with one side of the kissing loop or stem, the individual twist angle variations of one stem become 12–30% greater than the other stem. The unmodified X-ray structure, $S_{271.273}$ (NMR) and N_{stems} (NMR) structures correspond to this case.

3.3. Principal component analysis (PCA)

The details of the dynamics of the unmodified and the modified kissing loop complexes are identified by applying principal component analysis (PCA) (i.e., essential dynamics) [36]. Eigenvectors are calculated from the covariance matrix of a MD trajectory and filtered along each eigenvector. Larger variance motions of the macromolecules can be captured in the lower frequencies with larger eigenvalues [37]. The first three eigenvectors derived from the trajectories of the unmodified and modified dodecamers account for more than 70% of the motion. In the case of the unmodified and modified kissing loop complexes (both X-ray and NMR), the first three eigenvectors account for more than 60% of the motions.

In the RNA dodecamer, the first few principal components (PC) in the north and south dodecamers have similar motions compared to those of the unmodified dodecamer. However, the magnitude of the motions in the north modified dodecamers are observed to be smaller than that of the unmodified dodecamer, which implies smaller variance due to the constrained sugars.

On the other hand, PCA results for the HIV-1 kissing loop complexes are more complicated than the dodecamer. Since the first principal component (PC1) has the largest variance of motion, vector components of PC1 are attached to each phosphate (P) and C4′ atom to visualize the direction and magnitude of the corresponding motion in Fig. 6. PC1 in Fig. 6(a) shows that the base pairs A_{272} and A_{280} behave like a hinge, which causes larger swing motions in stem-1 of the unmodified kissing loop complex. For PC2, the overall motions are uniform. For PC3, stem-1 has larger displacements compared to that of stem-2, and the motion of the kissing loop region is different for each stem. In the unmodified NMR structure, two symmetric bulged-in bases (A_{270} and A_{270}*) cause the overall motion in PC1 to be symmetric (see Fig. 6(b)). For PC2, stem-2 has larger motions than stem-1 due to the hydrogen bonds forming and breaking between A_{272}* and A_{280}*. The overall motion in PC3 also shows asymmetric behavior.

In the $N_{271.273}$ (X-ray), all flanking bases bulge-out and the symmetric base pairs of G_{271}–C_{281} and G_{271}*–C_{281}* behave like a hinge and each stem swings symmetrically in PC1 (see Fig. 6(c)) and PC2. For PC3, the motion near the 5′ and 3′ end of stem-1 is larger than the corresponding region of stem-2. In $N_{271.273}$ of the NMR structure where all flanking bases are bulged-out, all of PC1-PC3 motions are found to be very symmetric. In the X-ray $S_{271.273}$, base pairs G_{271}–C_{281} and G_{271}*–C_{281}* behave like a hinge and both stems swing symmetrically in PC1 (see Fig. 6(e)). However, since the two flanking bases bulge-out while the other two fluctuate between half bulged-in and bulged-out, stem-1 has larger motion than stem-2 in PC2 and the overall motion is asymmetric in PC3. In the NMR $S_{271.273}$, the three flanking bases (A_{272}*, A_{273}* and A_{272}) which are bulged-in and form hydrogen bonds inside the kissing loop complex cause the helical axis of stem-1 to be bent with respect to a coaxial axis. Due to the helical distortion, motions in PC1-PC3 are all asymmetric. Therefore, the conformation of the flanking bases determines the symmetry (direction and magnitude) of the motion between the stems.

Since A_{272} and A_{273} in the X-ray structure of N_{stems} bulge-out and stack, stem-1 has more freedom to move and PC1 in Fig. 6(g) shows larger motion in stem-1 than stem-2. However, both PC2 and PC3 show symmetric motion for the overall structure. In the N_{stems} NMR, in spite of A_{272}, A_{272}* and A_{273} staying in a bulged-in conformation while A_{273}* is bulged-out, the overall motion of PC1 is symmetric in both stems. Due to the wild motion of A_{273}*, PC2 shows that stem-1 has a larger displacement than stem-2. Uniform motion between stems was observed in PC3. Therefore, the symmetry of PC1-PC3 in N_{stems} is less affected by the flanking base conformations.

The degree of symmetry in PC1–PC3 for each case and the corresponding RMSD values are listed in Table 4. As symmetric motions are dominant for lower PCs ($N_{271.273}$ and N_{stems} of both the X-ray and the NMR structures), the corresponding structures have lower RMSDs. However, when asymmetric motions are dominant

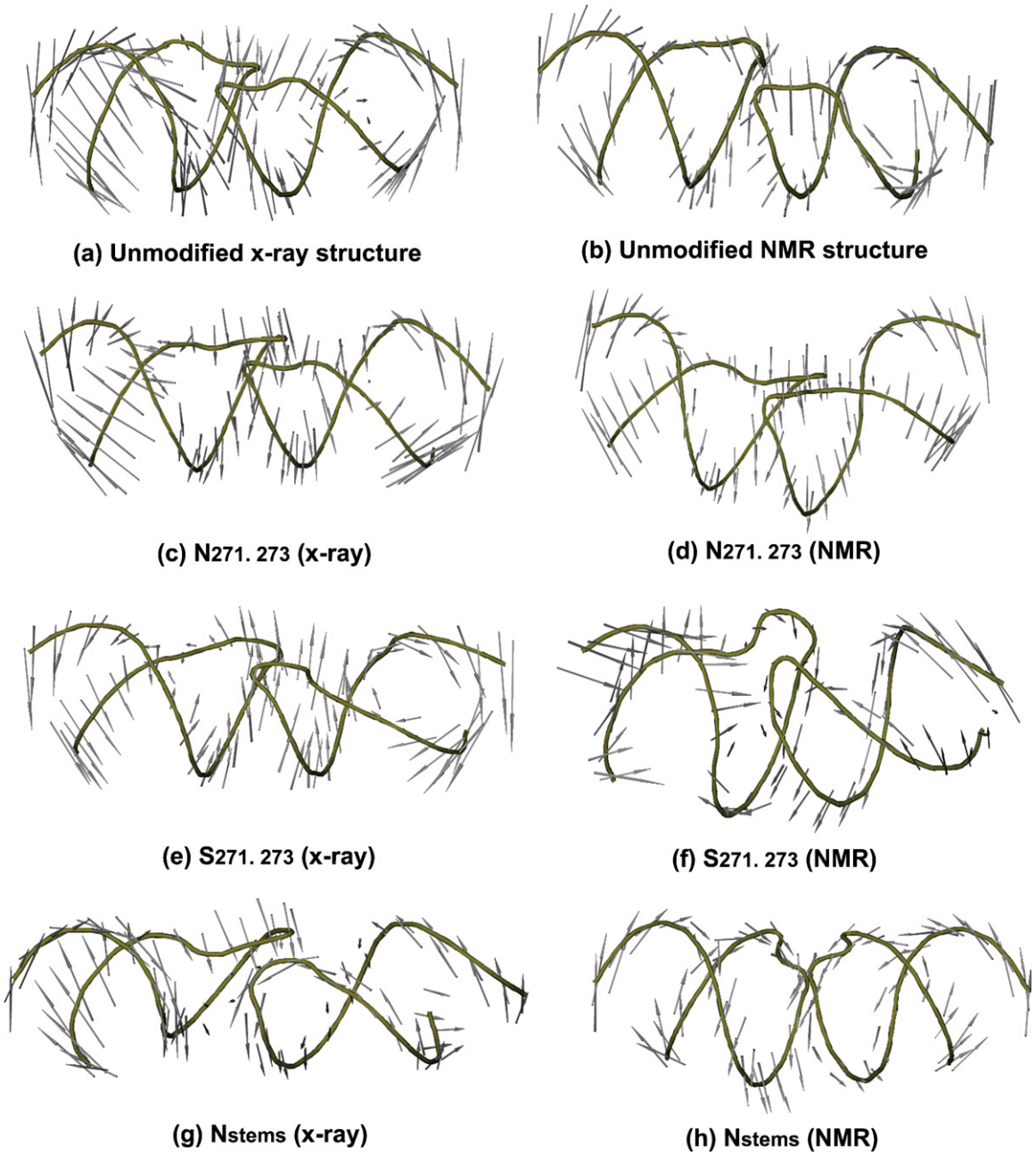

Fig. 6. Porcupine plots of the first principal component (PC1): (a) unmodified X-ray, (b) unmodified NMR, (c) $N_{271.273}$ (X-ray), (d) $N_{271.273}$ (NMR), (e) $S_{271.273}$ (X-ray), (f) $S_{271.273}$ (NMR), (g) N_{stems} (X-ray) and (h) N_{stems} (NMR).

Table 4
Summary of PC1-PC3 of the unmodified and modified kissing loop complexes.

Type	X-ray				NMR			
	Unmodified	$N_{271.273}$	$S_{271.273}$	N_{stems}	Unmodified	$N_{271.273}$	$S_{271.273}$	N_{stems}
PC1	A	S	S	A	S	S	A	S
PC2	S	S	A	S	A	S	A	A
PC3	A	A	A	S	A	S	A	S
RMSD(Å)	5.5 ± 1.5	3.0 ± 0.8	3.4 ± 0.6	3.1 ± 0.6	4.6 ± 0.8	2.4 ± 0.4	4.2 ± 0.8	3.0 ± 0.6

"A" and "S" indicate asymmetric and symmetric motions between stems of the kissing loop structure. Symmetry in motion is determined by porcupine plots (direction and magnitude) and the motion of each PC for the last 20 ns of MD simulation. When the dynamics have more symmetric motions, the RMSD values are smaller.

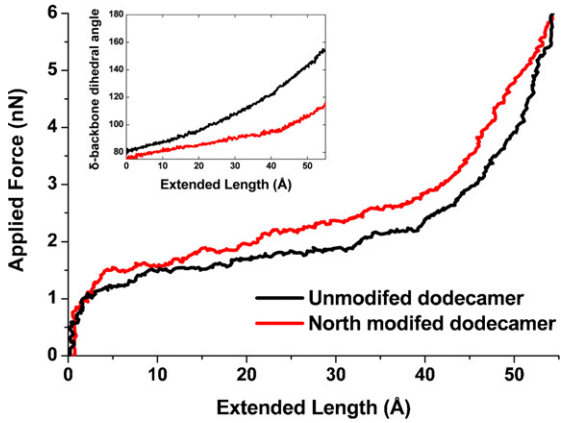

Fig. 7. The average force–extension curves of unmodified (black line) and north modified (red line) dodecamers. The inset is the variation of δ angle as a function of elongated length.

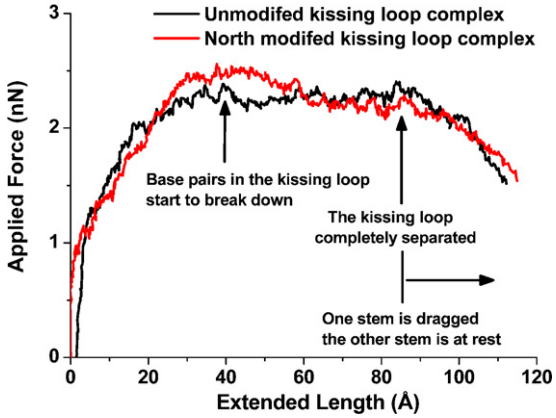

Fig. 8. The average force–extension curves of unmodified (black line) and north modified (red line) HIV-1 kissing loop complexes.

for lower PCs ($S_{271.273}$), the corresponding structures have relatively high RMSDs.

3.4. Steered molecular dynamics (SMD)

3.4.1. SMD of RNA dodecamer

Principal component analysis in the previous section shows the effect of substituted modified nucleotides on the overall dynamics for the first few eigenvectors, which contain most of the variance in motions. In order to examine the physical change due to the modifications, such as increased stiffness due to the constrained sugars, we apply steered molecular dynamics to the RNA dodecamers and the HIV kissing loop complexes. Fig. 7 shows the average force–extension curves for the unmodified and the north modified RNA dodecamers with respect to the extended length. The force–extension curve shapes in the RNA dodecamers are similar to that of DNA [38]. A flat force distribution between 5 and 40 Å is an overstretching region where a double strand force–extension curve transitions to that of a single strand. As both structures are elongated, larger force is applied to the modified dodecamer. When the elongation reaches 55 Å, the average δ angle in the unmodified dodecamer increases 33° more than that of the modified dodecamer (see the inset of Fig. 7). Therefore, the increased resistance to change of the backbone δ angles associated with the constrained sugars requires more force to elongate the north dodecamer. In addition, due to the relatively smaller deformations in the sugar puckers, the change of average χ angles in the north modified dodecamer is 22° less than that of the unmodified. On the other hand, other backbone dihedral angles compensate for the smaller changes in the δ angle. When the elongated lengths of both dodecamers reach 55 Å, the average β and ζ angles between the north modified and the unmodified dodecamer show 12° and 22° differences respectively, while other backbone angles (α, γ and ε) remain the same.

3.4.2. SMD of HIV-1 kissing loop complex

Since it is found that the overall stability in N_{stems} is independent of the flanking base conformations, SMD is applied to N_{stems} (X-ray) for further analysis. The extension of the HIV kissing loop complexes under the applied force is plotted in Fig. 8. The force–extension curve has three different regions in terms of extension length. From the beginning to 40 Å, the external force increases, and over the range of 40–80 Å, the external force becomes flat. Beyond 80 Å, the external force applied to both the unmodified and the modified kissing loop starts to decrease. In the first region, both stems are elongated by the applied external force. In the second region, the outer base pairs in the loop start to break down first. In the unmodified kissing loop complex, C_{279}–G_{274}*, C_{274}–G_{279}* and C_{278}–G_{275}* pairs start to break down at 47, 58, and 64 Å respectively. The remaining three base pairs, C_{275}–G_{278}*, C_{277}–G_{276}*, and C_{276}–G_{277}* break down in the range of 76–80 Å. In the modified kissing loop complex, both C_{274}–G_{279}* and C_{279}–G_{274}* pairs break down at 51 Å and then both C_{275}–G_{278}* and C_{278}–G_{275}* pairs break down at 70 Å. The remaining two base pairs break down at 75 and 80 Å respectively. Beyond 80 Å, the hairpin loops of the unmodified and the modified kissing loop complexes are completely separated and one of the stems is dragged by the external force, while the other is at rest.

The applied force in the modified kissing loop complex is slightly higher than the unmodified between 20 and 60 Å. Beyond 60 Å, the force–extension curves of the two kissing loop complexes become the same. Since the north modified nucleotides are substituted into stems, the average backbone angles in stems and loop regions are calculated separately. When the elongation reaches 80 Å, the average δ angle in the unmodified kissing loop stems increases to 116°, while that of the modified kissing loop complex increases to only 90°. The average χ angle in the modified kissing loop stems is also 15° less than that of the unmodified kissing loop stems. The changes of other backbone angles between two kissing loop complexes are smaller than 6°. On the other hand, the backbone angle change of the loop region shows different behavior. The differences in the averages of the α, β, δ and χ angles between two kissing loop complexes are less than 3°, while the other backbone angles, ε, γ and ζ show larger than 10° differences. Therefore, the deformation patterns under applied force are different between the unmodified and the modified kissing loop complexes. The change in δ and χ angles indicates that the modified kissing loop complex is stiffer than the unmodified. Due to the higher stiffness in the modified kissing loop complex, base pairs in the loop break down simultaneously, while those in the unmodified kissing loop complex break down in a sequential fashion.

4. Conclusions

In developing RNA based nanoparticles, it is expected that substituting north and south constrained sugars into selected positions can control system stiffness and shape. Our results show that there are various possibilities for the use of constrained sugars in RNA nanoparticle design. The dynamic behavior of the north dodecamer does not show any significant deviation from the unmodified RNA dodecamer. However, it is found that the stiffness of the north dodecamer increases significantly as measured by the SMD simulation.

On the other hand, the south modified dodecamer has both A and B-form backbone angles. In addition, the total length of the helix elongates and the overall twist angle is reduced compared to the unmodified dodecamer.

In the HIV kissing loop complex, the sugar puckers in G_{271}, G_{272} and A_{273} in the X-ray structure are south–north–south conformations, while those of the NMR structure are north–south–north conformations. Substituting modified nucleotides into flanking bases does not deform the X-ray structure to the NMR structure or vice versa. As shown in Table 3, substituting south constrained sugars at G_{271} and A_{273} in the NMR structure does not induce the flanking base conformation and the overall dynamics to those of the X-ray structure. The north constrained sugars at G_{271} and A_{273} in the X-ray structure also do not match the flanking base conformation and overall dynamics of the NMR structure. However, each group of modified kissing loop complexes shows consistent behaviors between the X-ray and NMR structures. During the MD simulations, one flanking base in the X-ray and two flanking bases in the NMR structures of the unmodified kissing loop complexes form a bulged-in conformation. The substitution of the north modified nucleotides at G_{271}, A_{273} ($N_{271.273}$) induce all flanking bases in both the X-ray and the NMR structures to a bulged-out and stacked (closed conformation). However, the south modified nucleotides at the same positions ($S_{271.273}$) fail to induce a closed conformation for both the X-ray and the NMR structures. Therefore, the type and position of substituted modified nucleotides control the flanking base formations regardless of their initial structures. In addition, the modified kissing loop complex, $N_{271.273}$ (both X-ray and NMR) show the most stable dynamics in terms of RMSD and PCA. $S_{271.273}$, however, shows less improvement in RMSD and asymmetric motions in PCA. When all nucleotides in both stems are replaced with north constrained sugars (N_{stems}), the overall RMSD is significantly decreased regardless of the flanking base conformations and the flexibility of the twist motion is the same as the unmodified kissing loop complex. The force–extension curves of the dodecamer and the kissing loop complexes show different behaviors due to the kissing loop breaking down during the extension of the kissing loop complex. However, both results show that the use of constrained sugars increases the stiffness of RNA structures associated with the resistance against deformation.

In conclusion, our research shows that the modified kissing loop complex can be used to stabilize the dynamics of RNA nanoparticle motifs and increase their stiffness. Since the substituted modified nucleotides can alter the overall twist angle and flexibility of the kissing loop complex, it can enhance or prohibit nanoparticle assembly such as tectosquares and RNA hexagonal nanorings.

Acknowledgements

We would like to thank Igor Topol for the valuable discussions regarding the ab initio calculations. This research was supported by the Intramural Research Program of the National Institutes of Health (NIH), National Cancer Institute (NCI), Center for Cancer Research Nanobiology Program (CCRNP). The computational support was provided by the National Cancer Institute's Advanced Biomedical Computing Center (ABCC).

References

[1] S. Hoeprich, Q. Zhou, S. Guo, D. Shu, G. Qi, Y. Wang, P. Guo, Bacterial virus phi29 pRNA as a hammerhead ribozyme escort to destroy hepatitis B virus, Gene Ther. 10 (2003) 1258–1267.
[2] A. Chworos, I. Severcan, A.Y. Koyfman, P. Weinkam, E. Oroudjev, H.G. Hansma, L. Jaeger, Building programmable jigsaw puzzles with RNA, Science 306 (2004) 2068–2072.
[3] Y.G. Yingling, B.A. Shapiro, Computational design of an RNA hexagonal nanoring and an RNA nanotube, Nano Lett. 7 (2007) 2328–2334.
[4] K.A. Afonin, E. Bindewald, A.J. Yaghoubian, N. Voss, E. Jacovetty, B.A. Shapiro, L. Jaeger, In vitro assembly of cubic RNA-based scaffolds designed in silico, Nat. Nanotechnol. 5 (2010) 676–682.
[5] M. Paliy, R. Melnik, B.A. Shapiro, Molecular dynamics study of the RNA ring nanostructure: a phenomenon of self-stabilization, Phys. Biol. 6 (2009) 046003.
[6] E. Bindewald, C. Grunewald, B. Boyle, M. O'Connor, B.A. Shapiro, Computational strategies for the automated design of RNA nanoscale structures from building blocks using NanoTiler, J. Mol. Graph. Model. 27 (2008) 299–308.
[7] E. Bindewald, R. Hayes, Y.G. Yingling, W. Kasprzak, B.A. Shapiro, RNAJunction: a database of RNA junctions and kissing loops for three-dimensional structural analysis and nanodesign, Nucl. Acids Res. 36 (2008) D392–D397.
[8] V. Pande, L. Nilsson, Insights into structure, dynamics and hydration of locked nucleic acid (LNA) strand-based duplexes from molecular dynamics simulations, Nucl. Acid Res. 36 (2008) 1508–1516.
[9] J.B. Rodriguez, V.E. Marquez, M.C. Nicklaus, J.J. Barchi Jr., Synthesis of cyclopropane-fused dideoxycarbocyclic nucleosides structurally related to neplanocin C, Tetrahedron Lett. 34 (1993) 6233–6236.
[10] J.B. Rodriguez, V.E. Marquez, M.C. Nicklaus, H. Mitsuya, J.J. Barchi Jr., Conformationally locked nucleoside analogues. Synthesis of dideoxycarbocyclic nucleoside analogues structurally related to neplanocin C, J. Med. Chem. 37 (1994) 3389–3399.
[11] K.H. Altmann, R. Kesselringa, E. Francotteb, G. Rihsc, 4′,6′-Methano carbocyclic thymidine: A conformationally constrained building block for oligonucleotides, Tetrahedron Lett. 35 (1994) 2331–2334.
[12] K.H. Altmann, R. Imwinkelrieda, R. Kesselringa, G. Rihsb, 1′′,6′′-methano carbocyclic thymidine: Synthesis, X-ray crystal structure, and effect on nucleic acid duplex stability, Tetrahedron Lett. 35 (1994) 7625–7628.
[13] A. Ezzitouni, J.J. Barchi Jr., V.E. Marquez, A simple approach to 1′′,1′′a-methano carbocyclic, Thymidine, Chem. Commun. 13 (1995) 1345–1346.
[14] M.A. Siddiqui, A. Ford Jr., C. George, V.E. Marquez, Synthesis, Conformational analysis, and biological activity of a rigid carbocyclic analogue of 2'-Deoxy Aristeromycin Built on a Bicyclo[3.1.0]hexane Template, Nucleosides Nucleotides 15 (1996) 235–250.
[15] A.T. Macias, N.K. Banavali, A.D. MacKerell Jr., DNA bending induced by carbocyclic sugar analogs constrained to the north conformation, Biopolymers 85 (2007) 438–449.
[16] Z. Wu, M. Maderia, J.J. Barchi Jr., V.E. Marquez, A. Bax, Changes in DNA bending induced by restricting nucleotide ring pucker studied by weak alignment NMR spectroscopy, Proc. Natl. Acad. Sci. U. S. A. 102 (2005) 24–28.
[17] R. Wing, H. Drew, T. Takano, C. Broka, S. Tanaka, K. Itakura, R.E. Dickerson, Crystal structure analysis of a complete turn of B-DNA, Nature 287 (1980) 755–758.
[18] L.M. Wadley, K.S. Keating, C.M. Duarte, A.M. Pyle, Evaluating and learning from RNA pseudotorsional space: quantitative validation of a reduced representation for RNA structure, J. Mol. Biol. 372 (2007) 942–957.
[19] V.E. Marquez, M.A. Siddiqui, A. Ezzitouni, P. Russ, J. Wang, R.W. Wagner, M.D. Matteucci, Nucleosides with a twist. Can fixed forms of sugar ring pucker influence biological activity in nucleosides and oligonucleotides? J. Med. Chem. 39 (1996) 3739–3747.
[20] P. Wang, A.S. Brank, N.K. Banavali, M.C. Nicklaus, V.E. Marquez, J.K. Christman, A.D. MacKerell Jr., Use of oligodeoxyribonucleotides with conformationally constrained abasic sugar targets to probe the mechanism of base flipping by HhaI DNA (Cytosine C5)-methyltransferase, J. Am. Chem. Soc. 122 (2000) 12422–12434.
[21] K. Bondensgaard, M. Petersen, S.K. Singh, V.K. Rajwanshi, R. Kumar, J. Wengel, J.P. Jacobsen, Structural studies of LNA:RNA duplexes by NMR: conformations and implications for RNase H activity, Chemistry 6 (2000) 2687–2695.
[22] K.E. Nielsen, S.K. Singh, J. Wengel, J.P. Jacobsen, Solution structure of an LNA hybridized to DNA: NMR study of the d(CT(L)GCT(L)T(L)CT(L)GC):d(GCAGAAGCAG) duplex containing four locked nucleotides, Bioconjug. Chem. 11 (2000) 228–238.
[23] M. Petersen, K. Bondensgaard, J. Wengel, J.P. Jacobsen, Locked nucleic acid (LNA) recognition of RNA: NMR solution structures of LNA:RNA hybrids, J. Am. Chem. Soc. 124 (2002) 5974–5982.
[24] K.E. Nielsen, J. Rasmussen, R. Kumar, J. Wengel, J.P. Jacobsen, M. Petersen, NMR studies of fully modified locked nucleic acid (LNA) hybrids: solution structure of an LNA:RNA hybrid and characterization of an LNA:DNA hybrid, Bioconjug. Chem. 15 (2004) 449–457.
[25] B. Wang, K.M. Merz Jr., A Fast QM/MM (Quantum Mechanical/Molecular Mechanical) approach to calculate nuclear magnetic resonance chemical shifts for macromolecules, J. Chem. Theory Comput. 2 (2006) 209–215.
[26] M.J. Frisch, G.W. Trucks, H.B. Schlegel, G.E.Scuseria, M.A. Robb, et al., Gaussian 03, Revision C.02, Wallingford, CT, 2004, Gaussian, Inc.
[27] C.I. Bayly, P. Cieplak, W. Cornell, P.A. Kollman, A well-behaved electrostatic potential based method using charge restraints for deriving atomic charges: the RESP model, J. Phys. Chem. 97 (1993) 10269–10280.
[28] J. Wang, P. Cieplak, P.A. Kollman, How well does a Restrained Electrostatic Potential (RESP) Model perform in calculating conformational energies of organic and biological molecules? J. Comput. Chem. 21 (2000) 1049–1074.
[29] D.A. Case, T.A. Darden, T.E., Cheatham III, C.L. Simmerling, R.E. Wang, et al., AMBER 10, 2008, University of California, San Francisco.
[30] W.L. Jorgensen, J. Chandrasekhar, J.D. Madura, M.L. Klein, Comparison of simple potential functions for simulating liquid water, J. Chem. Phys. 79 (1983) 926–935.
[31] U. Essmann, L. Perera, M.L. Berkowitz, T. Darden, H. Lee, L.G. Pedersen, A smooth particle mesh Ewald method, J. Chem. Phys. 103 (1995) 8577–8593.

[32] J.P. Ryckaert, G. Ciccotti, H.J.C. Berendsen, Numerical integration of the cartesian equations of motion of a system with constraints: molecular dynamics of n-alkanes, J. Comput. Phys. 23 (1977) 327–341.
[33] H.J.C. Berendsen, J.P.M. Postma, W.F.v. Gunsteren, A. DiNola, J.R. Haak, Molecular dynamics with coupling to an external bath, J. Chem. Phys. 81 (1984) 3684–3690.
[34] R. Lavery, H. Sklenar, The definition of generalized helicoidal parameters and of axis curvature for irregular nucleic acids, J. Biomol. Struct. Dynam. 6 (1988) 63–91.
[35] K. Reblova, E. Fadrna, J. Sarzynska, T. Kulinski, P. Kulhanek, E. Ennifar, J. Koca, J. Sponer, Conformations of flanking bases in HIV-1 RNA DIS kissing complexes studied by molecular dynamics, Biophys. J. 93 (2007) 3932–3949.
[36] J. Mongan, Interactive essential dynamics, J. Comput. Aided Mol. Design 18 (2004) 433–436.
[37] M.M. Teeter, D.A. Case, Harmonic and quasiharmonic descriptions of crambin, J. Phys. Chem. 94 (1990) 8091–8097.
[38] M. Santosh, P.K. Maiti, Force induced DNA melting, J. Phys.: Condens. Matter 21 (2009) 1–8.
[39] N. Foloppe, A.D. MacKerell Jr., All-atom empirical force field for nucleic acids: I. Parameter optimization based on small molecule and condensed phase macromolecular target data, J. Comput. Chem. 21 (2000) 86–104.